Analyst

PAPER

View Article Online
View Journal

Cite this: DOI: 10.1039/c8an02441c

A fluorimetric nitrite biosensor with polythienothiophene-fullerene thin film detectors for on-site water monitoring†

Nuno Miguel Matos Pires,[a,b,c] Tao Dong *[b] and Zhaochu Yang[a]

A novel fluorimetric sensor for highly sensitive nitrite detection on the site is presented in this study. The proposed on-chip approach comprises the use of integrated polymer photodetectors to detect light from fluorescence reactions with a diaminofluorescein probe. The detectors were prepared with a heterostructured nanofilm of polythieno[3,4-*b*]thiophene/benzodithiophene and (6,6)-phenyl-C_{71}-butyric-acid methyl-ester as a photoactive layer. Prior to fluorimetric detection, the quality of the spin-coated photoactive layer was characterized *via* nano-morphology and current-density measurements. Nitrite assays were conducted on a poly(methyl methacrylate) microchannel chip, to which polythienothiophene-C_{71} based detectors were aligned. Results of signal-to-noise ratio determination have indicated a detection limit below 0.55 μM, lower than the 0.1 mg L^{-1} maximum limit of operation in recirculating aquaculture systems for farming Atlantic salmon *Salmo salar*. An increase of the nitrite concentration to toxic levels may therefore be possible to detect. The fluorimetric sensor exhibited good linearity over three orders of magnitude and acceptable detection reproducibility, which confirmed its analytical value. Further tests revealed great promise of the integrated biosensor device for detecting nitrite in aquaculture-relevant samples with high precision. The approach reported hereby may provide impetus to *in situ* analytical tools for monitoring water quality at aquaculture facilities, the food industries or water monitoring stations.

Received 17th December 2018,
Accepted 1st June 2019

DOI: 10.1039/c8an02441c

rsc.li/analyst

1 Introduction

Elevated concentrations of nitrite (NO_2^-) are particularly critical in a reducing water environment.[1–3] A recirculating aquaculture system (RAS) is a typical case of a reducing water environment, where uncontrolled levels of NO_2^- pose a risk of toxicity to farmed fish.[4,5] Toxic levels of NO_2^- in a RAS may result from the imminent failure or malfunction of the biofilter converting ammonia to nitrate. The principal consequence of NO_2^- accumulation is the oxidation of haemoglobin, making it impossible to bind oxygen molecules. The oxidized form of haemoglobin is named methaemoglobin, and severe methaemoglobinemia or "brown blood disease" can lead to reduced growth and even high mortality to fish.[6–8] In practice, NO_2^- is maintained below 1 mg L^{-1} concentrations for different fish species reared in water run in a commercial RAS.[9] Moreover, human exposure to elevated NO_2^- levels can incur noxious health problems including, among others, infant methaemoglobinemia, and cancer in the digestive tract due to the formation of carcinogenic nitrosoamines by the reaction of nitrite with proteins.[2,10,11] The guideline value of NO_2^- set by the World Health Organization (WHO) is 3 mg L^{-1} in water.[1]

The detection of NO_2^- in water has been conducted using several biosensors and analytical methods over the past few years. The detection techniques encompass, among others, chromatographic,[12,13] spectrophotometric,[14–16] electrochemical,[17–19] chemiluminescence,[20,21] and fluorimetric detection.[22–24] Although the recent progress in these techniques has demonstrated good detection sensitivities for nitrite, the fluorimetric detection still remains the technique with higher attractiveness due to its easy procedure, low detection limits, high selectivity and low-cost.[23] The fluorimetric sensor is based on the detection of fluorescence intensity changes *via* reactions with a fluorescent probe.[25,26]

[a]*Chongqing Key Laboratory of Micro-Nano Systems and Smart Transduction, Collaborative Innovation Center on Micro-Nano Transduction and Intelligent Eco-Internet of Things, Chongqing Key Laboratory of Colleges and Universities on Micro-Nano Systems Technology and Smart Transducing, National Research Base of Intelligent Manufacturing Service, Chongqing Technology and Business University, Nan'an District, Chongqing 400067, China*

[b]*Department of Microsystems – IMS, Faculty of Technology, Natural Sciences and Maritime Sciences, University of South-Eastern Norway-USN, P.O. Box 235, 3603 Kongsberg, Norway. E-mail: tao.dong@usn.no; Tel: +47 31009321*

[c]*Centre for Environmental Radioactivity (CERAD CoE), Norwegian University of Life Sciences (NMBU), Faculty of Environmental Sciences and Natural Resource Management, P.O. Box 5003, NO-1432 Ås, Norway*

†Electronic supplementary information (ESI) available. See DOI: 10.1039/c8an02441c

The analysis of the fluorescence intensity is acknowledged to be a valuable analytical procedure for water quality management in fish farms.[27] It has been used to rapidly measure proteins, chlorophyll or other organic compounds which, in combination with the traditional measurement of physicochemical parameters (*i.e.* temperature, conductivity, color, *etc.*), enables a more robust analysis of aquaculture water quality. Despite this, the spectrophotometric method is still the common method for NO_2^- detection in a RAS.[5,28,29] The used method involves the standard diazotization reaction of NO_2^-, coupled with absorbance measurements of a coloured product. Moreover, these absorbance measurements have been conducted using bench-top spectrophotometers,[28,29] which are currently obsolete in the market or still available with large dimensions and high-cost. Nevertheless, the fluorimetric technique so far applied to aquaculture water analysis still uses expensive and bulky fluorescence spectrometers, in which conventional photomultiplier tubes (PMTs) are incorporated.[27]

Inexpensive optical biosensors may find a great opportunity in the aquaculture field, where demands are increasing for low-cost *in situ* technology.[30] A way to ensure low-cost of optical biosensors is to integrate organic photodetectors (OPDs).[31,32] OPDs exhibit advantages over conventional PMTs or digital cameras in terms of versatility of fabrication and used materials, price, portability and compactness of the devices. OPDs can be fabricated by simple spin-coating or printing techniques, involving low temperature deposition of thin organic films. Moreover, the flexibility in the size and shape of the OPDs facilitates the optical alignment in microfluidic biosensors dedicated to chemiluminescence and fluorimetric detection.[33–35] Meanwhile, a biosensor integrating OPDs and a microfluidic chip can detect analytes utilizing only few volumes of samples and reagents, while retaining high detection sensitivity.[33,34] A typical device architecture of an OPD comprises an anode, an anode interfacial layer, a cathode, and a cathode interfacial layer, besides the photoactive layer. The simplicity of the OPD devices enhances the miniaturization and portability of biosensors. This type of biosensor would empower aquaculture producers with new tools for the analysis of NO_2^- or other important contaminants at the site.

The photoactive thin-film layer of the OPD determines the spectral response of the corresponding biosensor. It comprises n-type and p-type organic species, acting as electron donors and electron acceptors, and are deposited either with a layered structure (planar heterojunction, PHJ) or from a blend mixture (bulk heterojunction, BHJ). Both OPD types have been reported in microfluidic biosensors for fluorimetric detection, including PHJs of pentacene and fullerene-60 (C_{60}) or copper phthalocyanine (CuPc) and C_{60},[31,36] and BHJs of tris[4-(5-phenylthiopen-2-yl)phenyl]-amine (TPTPA) and fullerene-70 (C_{70}) or poly(3-hexylthiophene) (P3HT) and (6,6)-phenyl-C_{61}-butyric-acid methyl-ester ($PC_{60}BM$).[35,36] Recent advances in organic solar cell technology have revealed novel heterojunctions of superior quantum efficiency, such as the BHJs of polythieno[3,4-*b*]thiophene/benzodithiophene (PTB7):$PC_{70}BM$ or other heterojunctions of polythiophene derivatives and $PC_{70}BM$.[37,38] Despite the potentially high sensitivity, the PTB7:$PC_{70}BM$ OPD has not yet been demonstrated in biosensors. Moreover, there is a trend in OPD research towards "all-solution-processed" devices.[39] Therefore, while the anode interfacial layer is typically made of spin-coated poly(ethylenedioxythiophene):polystyrene sulphonate (PEDOT:PSS), the traditional Ca cathode interlayer shall be replaced by a solution-processed organic material.[40]

An integrated nitrite biosensor with PTB7:$PC_{70}BM$ OPDs is presented in this work. The OPDs with all-polymer interlayers were used to measure fluorescence signals, as a result of a nitrite assay with a diaminofluorescein-based probe. The fluorimetric assays were conducted on the surface of a transparent microfluidic chip, aligned to the OPD pixels of the photodetector chip. NO_2^- was detected to a submicromolar concentration, and the experimental results indicated the suitability of the novel biosensor in monitoring NO_2^- in aquaculture-relevant water samples. Furthermore, the obtained detection limit was comparable to those of other recently reported biosensors dedicated to nitrite detection.

2 Experimental

2.1 PTB7:$PC_{70}BM$ OPD with all-polymer interlayers

The detector was prepared on a glass substrate with pre-patterned indium tin oxide (ITO) anodes (100 nm thickness). The ITO/glass chip was cleaned with deionized (DI) water, acetone and isopropanol in sequential steps under sonication, and pre-treated with oxygen plasma (50 W, 6 min). The subsequent deposition processes of the polymer layers were conducted in a nitrogen-filled glove box. The anode interlayer made of 40 nm-thick PEDOT:PSS (Sigma-Aldrich, St Louis, MO, USA) was prepared onto ITO/glass *via* spin-coating, and dried at 150 °C. The deposition of the photoactive layer of PTB7:$PC_{70}BM$ (~100 nm thick) was followed by spin-coating from a solvent mixture. PTB7 and $PC_{70}BM$ (Sigma-Aldrich, both processed as received) were mixed with a concentration ratio of 10 mg L^{-1} to 15 mg L^{-1} in *o*-dichlorobenzene containing 1,8-diiodoctane (3% v/v). The cathode interlayer was made of linear polyethylenimine (L-PEI). A solution of 0.01 wt% L-PEI in methanol was spin-coated onto PTB7:$PC_{70}BM$, after pre-treatment of the BHJ.[39] Baking (90 °C, 15 min) was applied to the device following L-PEI deposition, and thermal vacuum evaporation was finally used to form the Al cathodes (100 nm thickness). The fabricated device was packaged using epoxy under UV light. Measurements with the PTB7:$PC_{70}BM$ OPD were performed using a 2600-type Keithley dual-channel source measure unit. The OPD was characterized under irradiation from a xenon lamp coupled with a standard AM1.5 global filter, for current density characterization, and a monochromatic light-source equipment for external quantum efficiency (EQE) determination. A white-light LED (Thorlabs Inc., Newton, NJ, USA) was also used for photocurrent characterization.

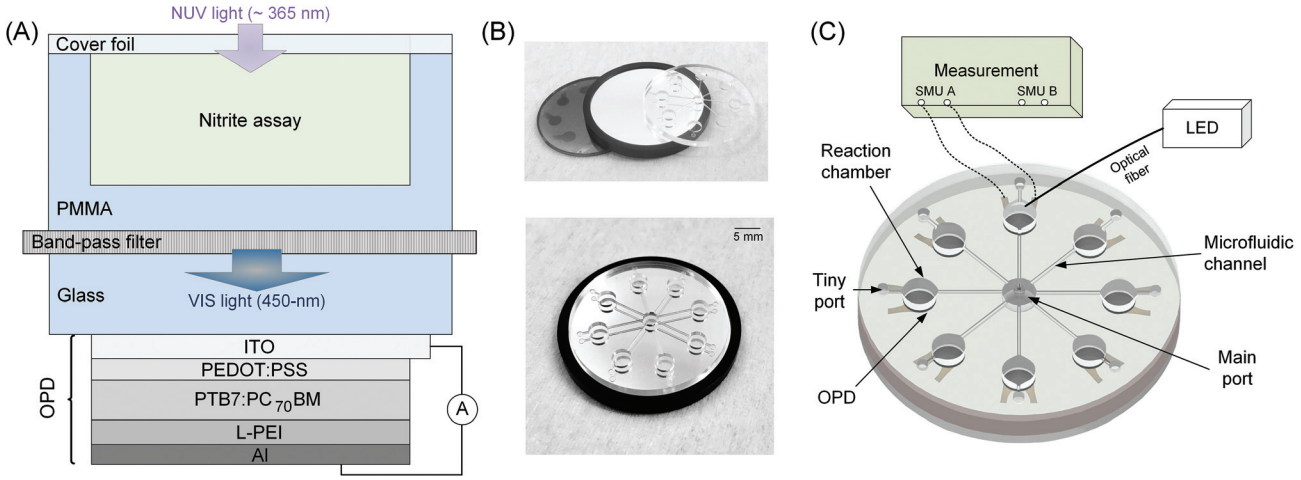

Fig. 1 Fluorimetric biosensor with PTB7:$PC_{70}BM$ OPDs integrated with a microfluidic chip. (a) Scheme of the integrated biosensor depicting a cross-section of the parts (layers not to scale). (b) Photographs of main device layers. (c) Scheme of the experimental setup for fluorescence measurements in a chamber. A representation of connections between the integrated biosensor and exterior is schematically presented. Abbreviations: NUV – near ultraviolet; VIS – visible; and LED – light emitting diode.

2.2 Microfluidic chip with functionalization

The transparent microfluidic chip was made of poly(methyl methacrylate) (PMMA). The chips were mainly processed by a precise CNC milling process. Different end milling cutters have defined the profile and fluidic structures of the PMMA chip. Fig. 1 shows the chip structures, including one main port (3 mm diameter, 1 mm depth), eight tiny ports (1 mm diameter), eight microchannels (4.5 mm length, 0.2 mm depth) and eight reaction chambers (~3.6 mm diameter).

The PMMA chips were cleaned with ethanol in an ultrasonic bath, and functionalized by pegylation prior to conducting the fluorimetric assays. Channels and chambers of the chips were pre-treated with oxygen plasma, and interacted with silane-poly(ethylene glycol) (Nanocs). Silane-poly(ethylene glycol) in stock solution was applied to the chips, and allowed to incubate at room temperature for a time not less than 30 min. The device was further rinsed with DI water to wash out the unreacted content, and later sealed with sterile pierceable cover foil (ThinSeal-type, EXCEL Scientific, Victorville, CA, USA). The treatment based on poly(ethylene glycol) was to enhance the surface hydrophilicity for the channels and chambers. Prior to fabrication and surface modification of the PMMA chips, the pegylated microfluidic structures were simulated with a finite element based simulation tool (COMSOL Multiplysics™).[41] Flow distribution along with dimensioning of the microfluidic structures were optimized with the software.

2.3 Fluorimetric detection apparatus and protocol

NO_2^- was detected in the reaction chambers of the PMMA chip. The fluorimetric assay utilized a diaminofluorescein-2 (DAF-2) probe[25] to obtain a highly fluorescent product (450 nm) in the presence of nitrite. For the assay, approximately 150 μL of a Measure-iT™ quantitation reagent (Invitrogen™ Molecular Probes™), previously diluted with DI water, were loaded to the chip, and allowed to enter the reaction chambers. Any excess of the quantitation reagent in the chambers was removed through the tiny ports. Furthermore, the sample was added to the chambers subjected to the test and incubated at room temperature. The assay was completed by adding a Measure-iT™ developer to the target chambers. The PMMA chip was subsequently aligned to the OPD-glass chip for the fluorescence measurements (see Fig. 1).

The increase in the fluorescence intensity due to NO_2^- detection was measured as the photocurrent with the OPDs. The glass chip containing the OPDs was placed onto a two-axis linear stage with rotating function, and a customized optical bandpass filter (ET 470/40x, Chroma Technology Co., VT, USA) was arranged between the glass chip and PMMA chip. A black-transparent sheet, with circular openings for the OPD active areas (~0.1 cm^2), was added to the glass surface opposite to the OPDs prior to the alignment of the parts. For the measurements, the excitation light from a 365 nm LED light source was directed to the center position of the reaction chamber using a standard optical fiber. The position of the OPD pixels was finely adjusted so as to ensure perfect alignment of the photoactive areas of the OPDs to the corresponding chambers of the PMMA chip. Fluorescent light passed through the pinholes of the black-transparent sheet reaching OPDs, while the sheet prevented interference from stray light. The detection of nitrite in one sample was conducted in duplicate reaction chambers, each one coupled with a LED and an OPD, with the photocurrent measured by the source measure unit. Recorded data were transferred from the source measure unit to a computer using a USB/GPIB interface adapter.

3 Results and discussion

3.1 Optoelectronic characterization

The fabricated OPD with the photodiode structure ITO/PEDOT:PSS/PTB7:$PC_{70}BM$/L-PEI/Al is shown in Fig. 1(a). The

polymer interlayers made of PEDOT:PSS and L-PEI were used to facilitate hole transport and electron transport, respectively, from the BHJ layer to the measuring electrodes. In particular, the L-PEI interlayer has replaced the traditional Ca-based electrode which is often associated with decreased device stability. Spin-coated L-PEI was hereby combined with the stable Al cathode, and the enhanced stability along with the enhanced use of spin-coating make these OPDs very interesting devices for *in situ* sensing with low cost. Furthermore, it has been shown in a previous study that no obvious degradation in performance was encountered with L-PEI cathodes in comparison with Ca analogues.[38]

The current–voltage (J–V) characteristics of the ITO/PEDOT:PSS/PTB7:$PC_{70}BM$/L-PEI/Al device are plotted in Fig. 2(a). Light detection was denoted by the significant difference in the measured current from tests in the dark to those conducted under irradiation from a visible-light simulator (xenon lamp with an AM1.5 filter). Approximately 14 mA cm^{-2} in current was obtained by operating the OPD with no bias voltage (short-circuit conditions), thereby indicating the sensitivity of the fabricated sensor to visible light. The high short-circuit current density (J_{sc}) is often associated with BHJ films of low surface roughness.[42] Atomic force microscopy (AFM) was utilized to characterize the topography of the fabricated BHJ film (see Fig. S1 in the ESI†). The film exhibited a homogeneous surface, with low roughness (root mean square of ~19 Å), which indicated the good quality of the fabricated BHJ. Moreover, from the measured J_{sc}, the EQE was determined as a function of the incident wavelength from a monochromatic light source.[34] The EQE exceeded 60% for wavelengths over 430 nm within the visible-light spectrum (Fig. 2(b)). This included the wavelength of 450 nm as the targeted wavelength to detect in the assays. The wide visible spectrum sensitivity of this OPD would also make it amenable for other fluorimetric assays[22,24,43] besides the nitrite detection method exploited in this work.

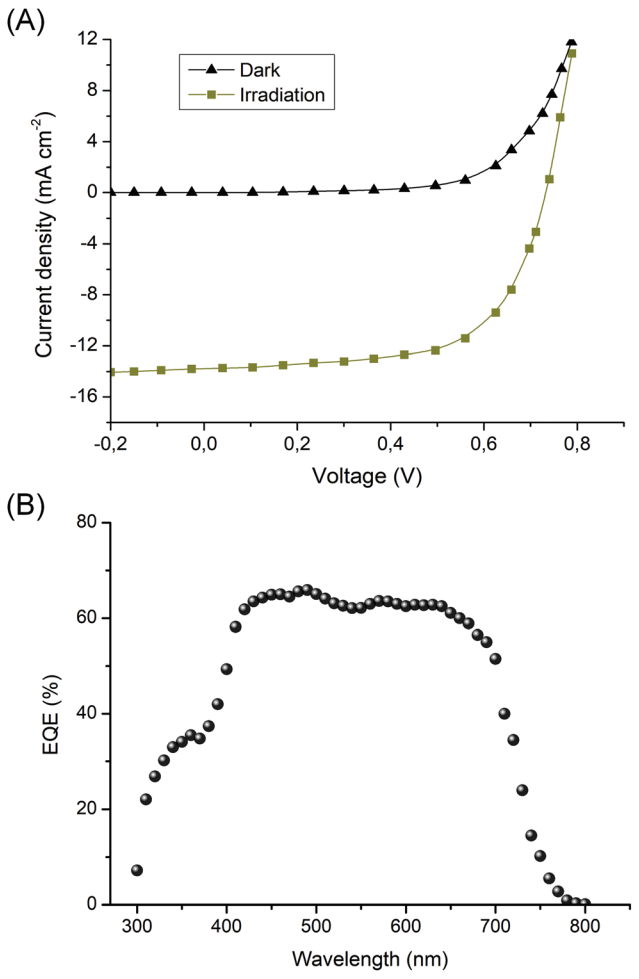

Fig. 2 Optoelectronic characterization of the PTB7:$PC_{70}BM$ OPD with all-polymer interlayers. (a) Current–voltage (J–V) response of the OPD under visible light irradiation and in the dark. (b) Spectral response of the fabricated OPD as a function of EQE to incident light wavelength.

The photocurrent response was also analysed before and after the PMMA microfluidic chip was modified with silane-poly(ethylene glycol). A white-light LED, with a peak luminescence near 450 nm, was employed to illuminate an OPD aligned below the microfluidic chip. There was no notable variation in the J_{sc} between illuminating pegylated and non-pegylated surfaces. Besides, the pegylation treatment introduced no significant effect to the background noise current of the OPD, thereby having no significant influence on the overall signal-to-noise ratio (SNR). Nevertheless, the poly(ethylene glycol) surface modifier conferred better wettability to the microfluidic channels and chamber surface. The silane terminals were decisive for the attachment of the poly(polyethylene glycol) modifier onto the PMMA surface, as silanes covalently bind to hydroxyl groups added to the surface after pre-treatment with oxygen plasma.[33]

3.2 Fluorimetric detection of nitrite

The first fluorimetric assays conducted with the pegylated PMMA chip and PTB7:$PC_{70}BM$ OPD chip were to estimate the lowest time necessary to achieve sensitive detection. The assays have targeted samples of 4.4 μM nitrite, and the fluorimetric measurements were performed applying reverse bias voltages to the photodetector. SNR responses are shown in Fig. 3(a), where the detection time corresponds to the time for sample incubation and addition of the developer. The photocurrent was measured immediately after adding the developer. The results suggested a detection time of 14 min to achieve a superior SNR, while the response of the biosensor did not significantly vary for greater detection times. Fig. 3(a) also shows the degradation in the SNR from applying a reverse bias. This observation was in agreement with the increase in the dark current of the OPD.

The biosensor exhibited a linear detection range of three orders of magnitude (in mg L^{-1}). The linear region of the biosensor response is plotted in Fig. 3(b). The limit of detection (LOD) was below 0.55 μM (~0.025 mg L^{-1}) as estimated from the 3× standard deviation of five blank measurements. The LOD is lower than 0.1 mg L^{-1} established as the

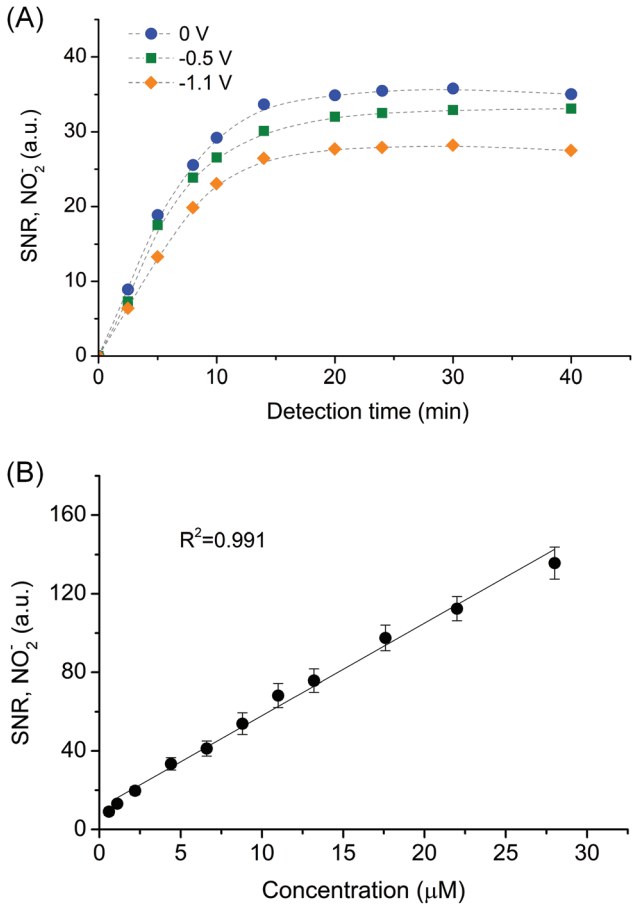

Fig. 3 Fluorimetric detection of nitrite with the PTB7:$PC_{70}BM$ OPD biosensor. (a) Detection of 4.4 μM NO_2^- as a function of the testing time and bias voltage applied to the OPD. (b) Dose–response curve depicting the linear range of NO_2^- detection with the fluorimetric biosensor. SNR corresponded to the ratio of the photocurrent due to nitrite detection to that measured with no sample. Calibration tests were performed in triplicate (n = 3).

maximum recommended value of NO_2^- in a RAS for rearing Atlantic salmon *Salmo salar*.[5,8] Moreover, the linear response of the biosensor covers NO_2^- concentrations in the range of 1 mg L^{-1}, which is an upper limit in RAS operations for farming other fish species besides A. salmon, such as tilapia or rainbow trout.[9] Therefore, the proposed sensor may eventually detect a dangerous increase of NO_2^- in RAS water, thereby preventing harmful effects to farmed fish. An uncontrolled increase of NO_2^- in the RAS may occur due to insufficient oxidation of ammonia during the nitrification process, or accumulation of nitrite in the system due to failure of the biofilter, among other factors affecting RAS operation.[4,7]

The detection limit achieved with the PTB7:$PC_{70}BM$ OPD was slightly lower than the LODs obtained with other organic photodetectors reported for fluorimetric detection, namely TPTPA:C_{70} (0.6 μM LOD) and P3HT:$PC_{60}BM$ (1 μM LOD).[35,36] These previous OPDs were also integrated with microfluidic chips demonstrating rapid bio-detection and low reagent consumption. Besides OPDs, other detectors such as charge-coupled devices (CCDs) have been employed for nitrite detection in microfluidic environments.[16,44] Two orders of magnitude for NO_2^- detection were achieved with the microfluidic device coupled to the CCD detector, while testing of the corresponding colorimetric detection approach was limited to a hundreds of μM range.[44] Moreover, the proposed biosensor showed an analytical performance in terms of the detection range, LOD and analysis time comparable to other fluorimetric sensors utilizing a PyI fluorescent probe (see Table 1). The fluorimetric assays for NO_2^- commonly require the use of bench-top fluorescence spectrometers; these instruments are very difficult to operate *in situ* due to their bulky dimensions, high cost, and need for specialized operators. Nevertheless, the miniaturization and low cost of the proposed biosensor are differential merits making it an attractive solution to aquaculture. Furthermore, the wide spectral response of the PTB7:

Table 1 Analytical performance for the detection of nitrite in water samples with the PTB7:$PC_{70}BM$ OPD biosensor and recently reported nitrite sensors

Detection range (μM)	LOD (μM)	Analysis time	Analytical technique	Detector	References
250–4000	<250	~90 s	Spectrophotometric assay in a microfluidic chip	CCD camera	Shi *et al.*[44]
1–20	0.1	Real-time	Spectrophotometric assay with Au-graphene oxide nanocomposites	UV-vis spectrometer	Amanulla *et al.*[14]
1.1–217	0.65	12 min	Spectrophotometric assay applying the Griess reagent in paper devices	Smartphone camera	Vidal *et al.*[46]
2–40	0.12	100 min	Spectrophotometric assay with a self-coupling diazotization reagent	UV-vis spectrometer	Wang *et al.*[47]
20–1000	1.06	A few seconds	Electrochemical detection with Au-graphene oxide nanocomposite	Glassy carbon electrode	Pan *et al.*[18]
2–425	0.7	<5 s	Electrochemical detection with a Ag-molybdenum disulfide nanocomposite	Carbon paste electrode	Ghanei-Motlagh and Taher[19]
5–1260	1.8	<5 s	Electrochemical detection with a Cu-carbon nanotube nanocomposite	Glassy carbon electrode	Manoj *et al.*[48]
0.025–20	0.009	5 min	Chemiluminescence with luminol and titanium oxide	Photomultiplier tube	Wang and Wang[45]
0–10	0.1	30 min	Fluorimetric detection with switch-off fluorescence probe PyI	Fluorescence spectrometer	Zhang *et al.*[11]
0.2–20	0.04	15 min	Fluorimetric detection with nitrogen-doped carbon quantum dots	Fluorescence spectrometer	Feng *et al.*[22]
0.1–100	0.05	Real-time	Fluorimetric detection with polymer-capped CdS quantum dots	Fluorescence spectrometer	Ren *et al.*[24]
1.1–28	<0.55	14 min	Fluorimetric detection in a microfluidic chip	OPD	This work

$PC_{70}BM$ OPD (430 to 650 nm) offers the possibility of exploiting other highly sensitive fluorescent probes, such as carbon quantum dots[22] or CdS quantum dots[23] which have been used for NO_2^- detection in water, or even exploiting ultra-sensitive chemiluminescence reactions of luminol in the presence of nitrite.[45]

Compared to other techniques for NO_2^- detection, the achieved LOD approximates to those of some recently reported spectrophotometric and electrochemical sensors (Table 1). In particular, on analyzing the analytical parameters listed in Table 1, it is found that the analytical performance of the PTB7:$PC_{70}BM$ OPD biosensor did not differ significantly from that exhibited by a spectrophotometric sensor employing the traditional Griess reagent onto micropapers.[46] Owing to its inherent simplicity and low cost, the paper-based approach may constitute another alternative to testing aquaculture water quality in the field. Nevertheless, it is worth noting that bulky and expensive UV-vis spectrometers have still been utilized in recent spectrophotometric sensors for NO_2^-.[14,47] With regard to the analysis time, the PTB7:$PC_{70}BM$ OPD biosensor tested the water sample in a time range of minutes, including sample incubation and measurement, which is in contrast to the analysis time of seconds as reported for electrochemical sensors.[18,48] Despite rapid detection, the electrochemical method is inherently vulnerable to variations of pH or ionic concentrations, which can affect the shelf life of the electrodes.[32] Moreover, the detection time of the proposed biosensor may prove to be sufficient for analyzing water samples *in situ*, as the standard methods of NO_2^- measurement in aquaculture water may take several hours (at least) from sampling to result measured in the laboratory.[28]

3.3 Precision of the PTB7:$PC_{70}BM$ OPD biosensor

The response of the PTB7:$PC_{70}BM$ OPD biosensor was further analysed using NO_2^- samples with concentrations below and above 0.1 mg L^{-1} (~2.17 μM), the limit value of NO_2^- for RAS farming A. salmon. Fig. 4(a) indicates the precision of the device in detecting nitrite in concentrations ranging from 1.7 μM to 5.5 μM. The detected concentrations were between reference values as obtained from the dose–response curve. The SNR value determined for 1.7 μM was higher than that for 1.1 μM and lower than that for 2.2 μM. The same consistency was found for the two other detected concentrations. The intra-assay variability was indicated by the relative standard deviation (RSD). The RSD has not exceeded 10.4%, 10.1%, and 8.2% for samples #1, #2, and #3, respectively. Nevertheless, these tests demonstrated the sensor ability to detect NO_2^- with acceptable accuracy.

The variability between different reaction chambers was also analysed. The SNR results of intra-assays plotted in Fig. 4(a) were obtained by testing each sample in two reaction chambers, as described in section 2.3. Fig. 4(b) shows the detection of samples#1 to #3 in four different chamber sets. Two sets were from a first PMMA chip, while the other two sets were tested from a second PMMA chip fabricated in the same batch. The SNR results from blank measurements (0 μM NO_2^-)

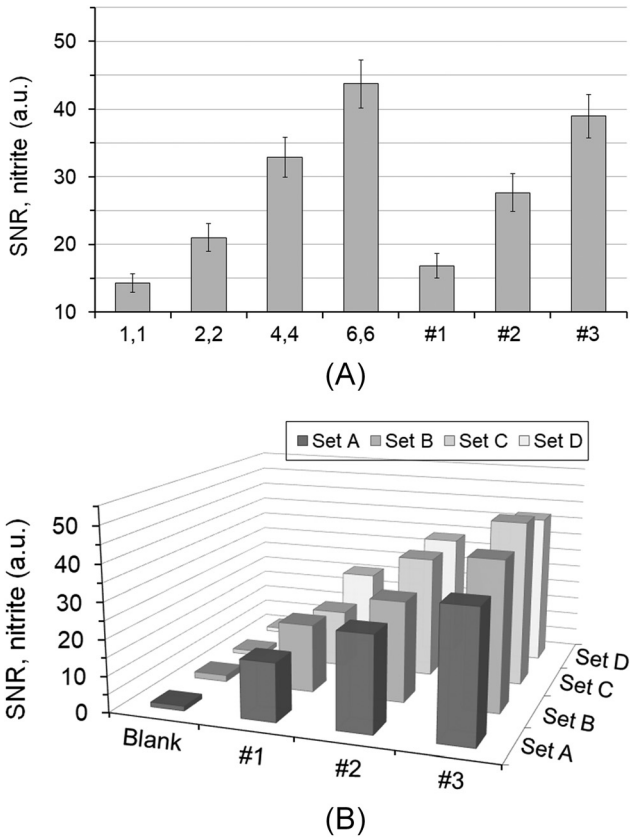

Fig. 4 Precision tests with the PTB7:$PC_{70}BM$ OPD biosensor. (a) SNR results from the detection of 1.7 μM, 3.5 μM and 5.5 μM NO_2^- samples marked as #1, #2, and #3, respectively. It also shows a plot of the SNR of four NO_2^- concentrations as obtained from the calibration. Detection tests were conducted in triplicate (n = 3). The x axis represents the concentration in μM. (b) 3D plot of SNR results from the detection of NO_2^- in four sets of reaction chambers. Sets A and B corresponded to four chambers in a first PMMA chip. Sets C and D were chamber sets from a second microfluidic chip.

are also plotted for comparison. All chamber sets consistently differentiated the concentrations of NO_2^- in samples#1 to #4. The inter-assay variability between the chamber sets did not exceed 11.6% for the detection of samples #1 to #3. The difference in the obtained SNR values can be explained by slight variations in photocurrent measurement and a slight variability introduced to the assays by possible operator errors. It is worth remarking that the use of PMMA chips with multiple reaction chambers was to make the inter-assay tests practical. The final biosensor would mainly require two zones, a blank zone for measuring the background noise and a detection zone to obtaining the photocurrent signal due to NO_2^- detection.

3.4 Detection of nitrite in aquaculture-relevant samples

The analysis of the analytical performance of the PTB7:$PC_{70}BM$ OPD biosensor was then extended to aquaculture-relevant water samples. Recent studies conducted on the characterization of a practical RAS have indicated the use of soft-

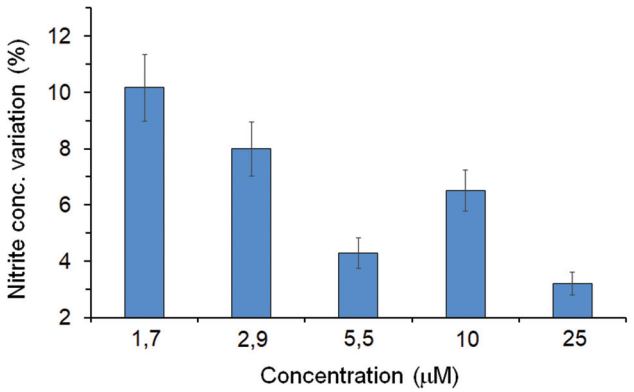

Fig. 5 Detection of nitrite in aquaculture background water. Detection tests of NO_2^- concentration were performed in triplicate (n = 3), RSD < 12%. The x axis of the plot represents the analyte concentration. The y axis marks the absolute percentage difference between the found concentration and original concentration.

hardness freshwater as a source in many RAS operations, as for A. salmon smolts.[29,49] In this work, synthetically prepared water with soft-hardness was used as a feasible approximation to a freshwater RAS. The preparation of this aquaculture background (AB) water is summarized in Table S1 (ESI†). Further detection experiments were conducted following addition of nitrite into AB water samples. The SNR value was first measured for each added NO_2^- concentration, and the found concentration was then estimated using the standard calibration curve obtained with AB water (see Fig. S2 in the ESI†). Fig. 5 plots the absolute percentage difference between the added and found NO_2^- concentrations. The results of the percentage difference ranged between 3.2 and 10.3% which corresponded to recoveries in the range of 92.05% to 110.3%, thus suggesting the suitability of the PTB7:PC_{70}BM OPD biosensor to detect nitrite in aquaculture-relevant water samples. Complementary tests of comparison between detecting nitrite in standard and AB water are shown in Fig. S3.†

The analytical device could be part of an alarm system signaling toxicity levels of NO_2^- in water from the RAS. The PTB7:PC_{70}BM OPD biosensor detected concentrations above the limits of 0.1 mg L^{-1} (~2.17 μM) and 1 mg L^{-1} (~21.7 μM) with high precision. Moreover, the precision of the method was also shown for low NO_2^- concentrations in real RAS water. The variability of seven measurements (n = 7) of 0.65 μM NO_2^- was below 10%. Besides the analytical performance, the simplicity and low-cost of the proposed biosensor enhance its usefulness for testing *in situ*. The device may test samples collected from the RAS water network, either from water exiting the biofilter or samples from the fish tank. Interestingly, the rapid detection of the increase in NO_2^- levels may provide an early-stage alarm of biofilter failure, therefore enabling the fish farmers to take fast remediation measures. Furthermore, the analytical device could also find an opportunity of application in monitoring other water samples such as drinking water.

4 Conclusions

A fluorimetric biosensor with PTB7:PC_{70}BM based photodetectors for NO_2^- detection in water is hereby shown. The biosensor attained good linearity, a low detection limit and acceptable reproducibility. The obtained detection range includes maximum NO_2^- limits of operation typically found in practical aquaculture systems for rearing A. salmon and other fish species. The characterized analytical performance was comparable to those of other recently reported nitrite sensors, including some spectrophotometric or fluorimetric sensors. Furthermore, the PTB7:PC_{70}BM photodetector had incorporated interfacial layers all made of polymers, thus following the development trend of OPD sensing technology while enhancing the low-cost of the photo-detection system and the resultant biosensor.

The analytical tests with aquaculture-relevant water samples further revealed the analytical usefulness of the PTB7:PC_{70}BM biosensing platform towards NO_2^- detection. The work presents an on-chip approach with low device complexity and low cost, which offers advantages over conventional bulky spectrometers envisaging the application *in situ*. Furthermore, the versatility of the biosensing platform may enable the detection of other toxic compounds besides nitrite in aquaculture water, utilizing other fluorescent probes. The approach may hold potential for analyzing other samples such as drinking water or even biological samples.

Conflicts of interest

There are no conflicts to declare.

Acknowledgements

The research was financed by the National Nature Science Foundation of China (Grant No. 61650410655), Research Council of Norway – HAVBRUK 2 program (Proj. no. 268017/E40), and RFF Oslofjordfondet (Proj. no. 285575 and 296654). The authors thank their colleague Simão Santos for assistance with AFM and support to fabrication and pre-characterization work. The support on water samples from Dr Hans-Christian Teien, and support to experiments from Luis Silva are appreciated. Assistance from Li Linbo and Han Xingyu is also acknowledged. The work has also received support from Chongqing Municipal Education Commission – Science and Technology Research Program (Proj. no. KJZD-K201800802 and KJ500609) and Chongqing Research Program of Basic Research and Frontier Technology (Proj. no. cstc2016jcyjA0292, cstc2017jcyjA1842 and cstc2018jcyjax0474).

References

1 World Health Organization, *Guidelines for Drinking-water Quality: incorporating first addendum*, WHO Press, Geneva, 2017.

2 R. I. Stefan-Van Staden, M. Mincu, J.(K.)F. van Staden and L. Gugoasa, Molecular recognition of nitrites and nitrates in water samples using graphene-based stochastic microsensors, *Anal. Chem.*, 2018, **90**, 9997–10000.
3 H. K. Kroupová, O. Valentová, Z. Svobodová, P. Sauer and J. Máchová, Toxic effects of nitrite on freshwater organisms: a review, *Rev. Aquacult.*, 2018, **10**, 525–542.
4 S.-Y. Zhang, G. Li, H.-B. Wu, X.-G. Liu, Y.-H. Yao, L. Tao and H. Liu, An integrated recirculating aquaculture system (RAS) for land-based fish farming: The effects on water quality and fish production, *Aquacult. Eng.*, 2011, **45**, 93–102.
5 B. F. Terjesen, S. T. Summerfelt, S. Nerland, Y. Ulgenes, S. O. Fjæra, B. K. M. Reiten, R. Selset, J. Kolarevic, P. Brunsvik, G. Bæverfjord, H. Takle, A. H. Kittelsen and T. Åsgård, Design, dimensioning, and performance of a research facility for studies on the requirements of fish in RAS environments, *Aquacult. Eng.*, 2013, **54**, 49–63.
6 F. B. Jensen, Nitrite disrupts multiple physiological functions in aquatic organisms, *Comp. Biochem. Physiol., Part A: Mol. Integr. Physiol.*, 2003, **135**, 9–24.
7 C. I. M. Martins, M. G. Pistrin, S. S. W. Ende, E. H. Eding and A. J. Verreth, The accumulation of substances in recirculating aquaculture systems (RAS) affects embryonic and larval development in common carp Cyprinus carpio, *Aquaculture*, 2009, **291**, 65–73.
8 H. Thorarensen and A. P. Farrell, The biological requirements for post-smolt Atlantic salmon in closed-containment systems, *Aquaculture*, 2011, **312**, 1–14.
9 J. Dalsgaard, I. Lund, R. Thorarinsdottir, A. Drengstig, K. Arvonen and P. B. Pedersen, Farming different species in RAS in Nordic countries: current status and future perspectives, *Aquacult. Eng.*, 2013, **53**, 2–13.
10 A. J. M. van Loon, A. A. M. Botterweck, R. A. Goldbohm, H. A. M. Brants, J. D. van Klaveren and P. A. van den Brandt, Intake of nitrate and nitrite and the risk of gastric cancer: a prospective cohort study, *Br. J. Cancer*, 1998, **78**, 129–135.
11 F. Zhang, X. Zhu, Z. Jiao, X. Liu and H. Zhang, Sensitive naked eye detection and quantification assay for nitrite by a fluorescence probe in various water resources, *Spectrochim. Acta, Part A*, 2018, **200**, 275–280.
12 D. Connolly and B. Paull, Rapid determination of nitrate and nitrite in drinking water samples using ion-interaction liquid chromatography, *Anal. Chim. Acta*, 2001, **441**, 53–62.
13 B. Zhu, Z. Zhong and J. Yao, Ion chromatographic determination of trace iodate, chlorite, chlorate, bromide, bromate and nitrite in drinking water using suppressed conductivity detection and visible detection, *J. Chromatogr. A*, 2006, **1118**, 106–110.
14 B. Amanulla, S. Palanisamy, S.-M. Chen, T.-W. Chiu, V. Velusamy, J. M. Hall, T.-W. Chen and S. K. Ramaraj, Selective colorimetric detection of nitrite in water using chitosan stabilized gold nanoparticles decorated reduced graphene oxide, *Sci. Rep.*, 2017, **7**, 14182.
15 A. R. Bertão, N. Pires, A. M. Fonseca, O. S. G. P. Soares, M. F. R. Pereira, T. Dong and I. C. Neves, Modification of microfluidic paper-based devices with dye nanomaterials obtained by encapsulation of compounds in Y and ZSM5 zeolites, *Sens. Actuators, B*, 2018, **261**, 66–74.
16 P. Singh, Y. R. Beg and G. R. Nishad, A review on spectroscopic methods for determination of nitrite and nitrate in environmental samples, *Talanta*, 2019, **191**, 364–381.
17 Y. Zhang, L. Luo, Y. Ding and L. Li, Electrochemical determination of nitrite in water samples using a glassy carbon electrode modified with didodecyldimethylammonium bromide, *Microchim. Acta*, 2009, **167**, 123–128.
18 F. Pan, D. Chen, X. Zhuang, X. Wu, F. Luan, S. Zhang, J. Wei, S. Xia and X. Li, Fabrication of gold nanoparticles/L-cysteine functionalized graphene oxide nanocomposites and application for nitrite detection, *J. Alloys Compd.*, 2018, **744**, 51–56.
19 M. Ghanei-Motlagh and M. A. Taher, A novel electrochemical sensor based on silver/halloysite nanotube/molybdenum disulfide nanocomposite for efficient nitrite sensing, *Biosens. Bioelectron.*, 2018, **109**, 279–285.
20 M. Yaqoob, B. F. Biot, A. Nabi and P. J. Worsfold, Determination of nitrate and nitrite in freshwaters using flow-injection with luminol chemiluminescence detection, *Luminescence*, 2012, **27**, 419–425.
21 L. F. B. A. da Silva, Z. Yang, N. M. M. Pires, T. Dong, H.-C. Teien, T. Storebakken and B. Salbu, Monitoring aquaculture water quality: design of an early warning sensor with Aliivibrio fischeri and predictive models, *Sensors*, 2018, **18**, 2848.
22 Z. Feng, Z. Li, X. Zhang, Y. Shi and N. Zhou, Nitrogen-doped carbon quantum dots as fluorescent probes for sensitive and selective detection of nitrite, *Molecules*, 2017, **22**, 2061.
23 Q.-H. Wang, L.-J. Yu, Y. Liu, L. Lin, R.-G. Lu, J.-P. Zhu, L. He and Z.-L. Lu, Methods for the detection and determination of nitrite and nitrate: a review, *Talanta*, 2017, **165**, 709–720.
24 H.-H. Ren, Y. Fan, B. Wang and L.-P. Yu, Polyethyleniminecapped CdS quantum dots for sensitive and selective detection of nitrite in vegetables and water, *J. Agric. Food Chem.*, 2018, **66**, 8851–8858.
25 M. Pereira, C. Soares, G. A. B. Canuto, M. F. M. Tavares, W. Colli and M. J. M. Alves, Down regulation of NO signaling in Trypanosoma cruzi upon parasite-extracellular matrix interaction: changes in protein modification by nitrosylation and nitration, *PLoS Neglected Trop. Dis.*, 2015, **9**, e0003683.
26 C.-G. Dai, J.-L. Wang, Y.-L. Fu, H. Zhou and Q.-H. Song, Selective and real-time detection of nitric oxide by a two-photon fluorescent probe in live cells and tissue slices, *Anal. Chem.*, 2017, **89**, 10511–10519.
27 C. S. M. Figueiró, D. Bastos de Oliveira, M. R. Russo, A. R. L. Caires and S. S. Rojas, Fish farming water quality monitored by optical analysis: The potential application of UV-VIS absorption and fluorescence spectroscopy, *Aquaculture*, 2018, **490**, 91–97.

28 J. Davidson, T. May, C. Good, T. Waldrop, B. Kenney, B. F. Terjesen and S. Summerfelt, Production of market-size North American strain Atlantic salmon Salmo salar in a land-based recirculation aquaculture system using freshwater, *Aquacult. Eng.*, 2016, **74**, 1–16.

29 C. Good, J. Davidson, B. F. Terjesen, H. Takle, J. Kolarevic, G. Bæverfjord and S. Summerfelt, The effects of long-term 20 mg/L carbon dioxide exposure on the health and performance of Atlantic salmon Salmo salar post-smolts in water recirculation aquaculture systems, *Aquacult. Eng.*, 2018, **81**, 1–9.

30 M. Saberioon, A. Gholizadeh, P. Cisar, A. Pautsina and J. Urban, Application of machine vision systems in aquaculture with emphasis on fish: state-of-the-art and key issues, *Rev. Aquacult.*, 2017, **9**, 369–387.

31 E. L. Ratcliff, P. A. Veneman, A. Simmonds, B. Zacher, D. Huebner, S. S. Saavedra and N. R. Armstrong, A planar, chip-based, dual-beam refractometer using an integrated organic light-emitting diode (OLED) light source and organic photovoltaic (OPV) detectors, *Anal. Chem.*, 2010, **82**, 2734–2742.

32 N. M. M. Pires, T. Dong, U. Hanke and N. Hoivik, Recent developments in optical detection technologies in lab-on-a-chip devices for biosensing applications, *Sensors*, 2014, **14**, 15458–15479.

33 N. M. M. Pires and T. Dong, Microfluidic biosensor array with integrated poly(2,7-carbazole)/fullerene-based photodiodes for rapid multiplexed detection of pathogens, *Sensors*, 2013, **13**, 15898–15911.

34 N. M. M. Pires and T. Dong, Integrated optical microfluidic biosensor using a polycarbazole photodetector for point-of-care detection of hormonal compounds, *J. Biomed. Opt.*, 2013, **18**, 097001.

35 Z. Shu, F. Kemper, E. Beckert, R. Eberhardt and A. Tunnermann, Highly sensitive on-chip fluorescence sensor with integrated fully solution processed organic light sources and detectors, *RSC Adv.*, 2017, **7**, 26384–26391.

36 R. Liu, R. Ishimatshu, M. Yahiro, C. Adachi, K. Nakano and T. Imato, Fluorometric flow-immunoassay for alkylphenol polyethoxylates on a microchip containing a fluorescence detector comprised of an organic light emitting diode and an organic photodiode, *Talanta*, 2015, **134**, 37–47.

37 M. Li, K. Gao, X. Wan, Q. Zhang, B. Kan, R. Xia, F. Liu, X. Yang, H. Feng, W. Ni, Y. Wang, J. Peng, H. Zhang, Z. Liang, H.-L. Yip, X. Peng, Y. Cao and Y. Chen, Solution-processed organic tandem solar cells with power conversion efficiencies >12%, *Nat. Photonics*, 2017, **11**, 85–90.

38 T. Dong and N. M. M. Pires, Immunodetection of salivary biomarkers by an optical microfluidic biosensor with polyethylenimine-modified polythiophene-C70 organic photodetectors, *Biosens. Bioelectron.*, 2017, **94**, 321–327.

39 F.-C. Wu, K.-C. Tung, W.-Y. Chou, F.-C. Tang and H.-L. Cheng, Charge selectivity in polymer: fullerene-based organic solar cells with a chemically linked polyethylenimine interlayer, *Org. Electron.*, 2016, **29**, 120–126.

40 C.-C. Chueh, C.-Z. Li and A. K.-Y. Jen, Recent progress and perspective in solution-processed interfacial materials for efficient and stable polymer and organometal perovskite solar cells, *Energy Environ. Sci.*, 2015, **8**, 1160–1189.

41 C. Honrado and T. Dong, Development and optimization of an integrated capillary-based opto-microfluidic device for chemiluminescence quantitative detection, *J. Micromech. Microeng.*, 2014, **24**, 125023.

42 Z. Ding, J. Kettle, M. Horie, S. W. Chang, G. C. Smith, A. I. Shames and E. A. Katz, Efficient solar cells are more stable: the impact of polymer molecular weight on performance of organic photovoltaics, *J. Mater. Chem. A*, 2016, **4**, 7274–7280.

43 J. Simões and T. Dong, Continuous and real-time detection of drinking-water pathogens with a low-cost fluorescent optofluidic sensor, *Sensors*, 2018, **18**, 2210.

44 Y. Shi, H. L. Liu, X. Q. Zhu, J. M. Zhu, Y. F. Zuo, Y. Yang, F. H. Jiang, C. J. Sun, W. H. Zhao and X. T. Han, Optofluidic differential colorimetry for rapid nitrite determination, *Lab Chip*, 2018, **18**, 2994–3002.

45 L. Wang and Q. Wang, Selective determination of nitrite/nitrate based on photo-induced redox activity of titanium dioxide, *J. Sep. Sci.*, 2018, **41**, 4075–4082.

46 E. Vidal, A. S. Lorenzetti, A. G. Lista and C. E. Domini, Micropaper-based analytical device (μPAD) for the simultaneous determination of nitrite and fluoride using a smartphone, *Microchem. J.*, 2018, **143**, 467–473.

47 H. Wang, N. Wan, L. Ma, Z. Wang, B. Cui, W. Han and Y. Chen, A novel and simple spectrophotometric method for detection of nitrite in water, *Analyst*, 2018, **143**, 4555–4558.

48 D. Manoj, R. Saravanan, J. Santhanalakshmi, S. Agarwal, V. K. Gupta and R. Boukherroub, Towards green synthesis of monodisperse Cu nanoparticles: An efficient and high sensitive electrochemical nitrite sensor, *Sens. Actuators, B*, 2018, **266**, 873–882.

49 T. Kristensen, Å. Åtland, T. Rosten, H. A. Urke and B. O. Rosseland, Important influent-water quality parameters at freshwater production sites in two salmon producing countries, *Aquacult. Eng.*, 2009, **41**, 53–59.